

# Shell-model study of spectroscopies and isospin structures in odd-odd $N = Z$ nuclei employing realistic $NN$ potentials

C. Qi<sup>1</sup> and F.R. Xu<sup>1,2,3,\*</sup>

<sup>1</sup>*School of Physics and MOE Laboratory of Heavy Ion Physics,  
Peking University, Beijing 100871, China*

<sup>2</sup>*Institute of Theoretical Physics, Chinese Academy of Sciences, Beijing 100080, China*

<sup>3</sup>*Center for Theoretical Nuclear Physics,  
National Laboratory for Heavy Ion Physics, Lanzhou 730000, China*

(Dated: February 9, 2020)

## Abstract

The structures of odd-odd  $N = Z$  nuclei in the lower  $fp$  shell have been investigated with a new isospin-nonconserving microscopical interaction. The interaction is derived from a high-precision charge-dependent Bonn nucleon-nucleon potential using the folded-diagram renormalization method. Excellent agreements with experimental data have been obtained up to band terminations. Particularly, the relative positions of  $T = 0$  and  $T = 1$  bands were well reproduced. Calculations with another interaction obtained from the Idaho-A chiral potential showed similar results. Our calculations also give a good description of the existence of high-spin isomeric states in the  $0f_{7/2}$  sub-shell. As examples, the spectroscopies and isospin structures of  $^{46}\text{V}$  and  $^{50}\text{Mn}$  have been discussed in detail, with the useful predictions of level structures including electromagnetic properties. Results for  $^{50}\text{Mn}$  were analyzed where experimental observations are still insufficient.

PACS numbers: 21.30.Fe, 21.60.Cs, 23.20.Lv, 27.40.+z

---

\*Electronic address: frxu@pku.edu.cn

## I. INTRODUCTION

Nuclei with the equal numbers of neutrons and protons ( $N = Z$ ) have become a special ground to investigate neutron-proton ( $np$ ) correlations. In  $N = Z$  nuclei, neutrons and protons occupy the same shell-model orbits, leading to large spatial overlaps between neutron and proton wave functions. The  $np$  pairing is further enhanced in odd-odd  $N = Z$  nuclei due to odd neutron and odd proton correlation. The  $np$  residual pairing interaction can be equally important as the neutron-neutron ( $nn$ ,  $T_z = 1, T = 1$ ) and proton-proton ( $pp$ ,  $T_z = -1, T = 1$ ) pairings. While  $nn$  and  $pp$  pairings have been well established in terms of the simple BCS model, the  $np$  pairing is still an open question that has motivated many recent theoretical and experimental works [1, 2, 3, 4, 5, 6, 7, 8, 9, 10, 11, 12, 13, 14, 15, 16, 17, 18].

In contrast to  $pp$  and  $nn$  correlations, the  $np$  pairing can form isovector ( $T_z = 0, T = 1$ ) and isoscalar ( $T_z = 0, T = 0$ ) configurations. The isovector channel manifest itself in a similar fashion to like-nucleon correlations, which can be evidenced with the presence of nearly degenerate  $T = 1$  isobaric triplets along the  $N = Z$  line [2]. The existence of the  $T = 0$  isoscalar component has also been shown theoretically, e.g., in Ref. [3]. In light  $N = Z$  nuclei, ground states usually favor the lowest  $T = 0$  isospin quantum number, while  $T = 1$  states appear at very high excitation energies. With increasing mass number, however,  $T = 0$  and  $T = 1$  bands begin to coexist at low excitation energies [1, 4]. In particular, the isospin structures of medium-mass  $fp$  shell nuclei are very interesting, where  $T = 1$  states can be lower than  $T = 0$  states.  $T = 1$  ground states have been expected systematically [4, 5].

Recent advances in experimental techniques enable us to study the structures of the odd-odd  $N = Z$  nuclei in the  $fp$  shell at high spins and high excitation energies. This provides an unique opportunity to investigate the interplay between  $T = 0$  and  $T = 1$  bands. Moreover, the high-precision measurements of level schemes provide useful information for discussion of the isospin asymmetry in their excited states at different angular momenta [6, 7, 8, 9, 10, 11, 12, 13, 14, 15]. Experimentally, isospin effects can be discussed by defining the mirror energy differences (MED) and triplet energy differences (TED) between analogous states in mirror pairs and  $T = 1$  triplets, respectively [19, 20, 21]. The differences have their origins from the Coulomb interaction and charge dependence in strong force, while the former usually plays a dominant role. In the  $fp$  shell, the coulomb shifts of single-

particle orbits are relatively small [21]. This allows us to extract the effect from the charge symmetry breaking in the strong force for the many-body systems of nuclei.

The purpose of this paper is to study the structures and properties of odd-odd  $N = Z$  nuclei in the  $fp$  model space by the shell-model diagonalization method. The many-body interaction used in the effective Hamiltonian has been derived from a high-precision charge-dependent Bonn (CD-Bonn) nucleon-nucleon ( $NN$ ) potential [22] using the so-called folded-diagram method [23]. The obtained interaction retains the charge-independence breaking effects in the  $NN$  potential. The contribution from the Coulomb field is also included. Hence the effective Hamiltonian does not conserve isospin.

In Section II, we describe briefly the folded-diagram method and the construction of the residual interaction. In Section III, the level structures of the odd-odd  $N = Z$  nuclei in the  $fp$  shell are calculated and discussed. In Section IV, we discuss the electromagnetic properties of the odd-odd  $N = Z$  nuclei with analyzing the isospin structures of the nuclei.

## II. EFFECTIVE INTERACTION

We start from the mean-field approximation with the perturbation expansion. In this approximation, it is convenient to reduce the degree of freedom of the Hilbert space for the many-fermion system of nuclei. For large-scale shell-model diagonalizations, the determination of the model space is a crucial step. The model space can be defined with the projection operator,

$$P = \sum_{i=1}^D |\Phi_i\rangle\langle\Phi_i|, \quad (1)$$

where  $D$  is the dimension of the model space, and wave functions  $|\Phi_i\rangle$  are eigenfunctions of the unperturbed Hamiltonian,  $H_0 = T + U$ , with  $T$  being the kinetic energy and  $U$  an appropriate one-body potential. The remaining space (so-called excluded space) can be expressed by

$$Q = \sum_{i=D+1}^{\infty} |\Phi_i\rangle\langle\Phi_i|. \quad (2)$$

The system of the full Hamiltonian with eigen energies  $E_\alpha$  and wave functions  $\Psi_\alpha$  that are determined by the full Schrödinger equation of  $H|\Psi_\alpha\rangle = E_\alpha|\Psi_\alpha\rangle$  can be reduced within the model space by projection [23],

$$PH_{\text{eff}}P|\Psi_\lambda\rangle = (E_\lambda - E_c)P|\Psi_\lambda\rangle = (E_\lambda - E_c)|\Phi_\lambda\rangle, \quad (3)$$

with  $E_\lambda \in \{E_\alpha\}$  ( $\lambda = 1, 2, \dots, D$ ) and  $E_c$  is the energy of the assumed core left behind in practical calculations.  $H_{\text{eff}}$  is the mode-space-dependent effective Hamiltonian. In the shell model context, the effective Hamiltonian can be decomposed into two parts,

$$H_{\text{eff}} = H'_0 + v_{\text{eff}}, \quad (4)$$

where  $H'_0 = \sum_\alpha \varepsilon'_\alpha a_\alpha^\dagger a_\alpha$  is the effective one-body Hamiltonian with  $\varepsilon'_\alpha$  being single-particle energies (SPE). The  $\varepsilon'_\alpha$  values can be obtained from the separation energies of valence particles. Usually, the effective interaction  $v_{\text{eff}}$  takes the form of pure two-body interactions. It can be expressed as two body matrix elements in harmonic oscillator (HO) basis.

The shell model provides the microscopic foundation to study the excitations of nuclei. The Cohen-Kurath [24] and universal SD (USD) [25] interactions have been proved to be quite successful and useful for the  $p$ - and  $sd$ - shell calculations, respectively. In past decades, extensive theoretical works have been conducted to improve the calculations of the shell model for  $0f_{7/2}$  nuclei in which exact diagonalizations have become possible due to the advance in computing techniques. The central spirit of shell model calculations is to find a unified interaction for a given mass region. For the  $fp$  nuclei, various interactions have been proposed, such as the Kuo-Brown (KB) renormalized G matrix [26] and its modified versions with monopole centroid corrections [27, 28], the FPD6 analytic two-body potential [29] and the GXPF interaction [30]. These interactions have been extensively tested with the successful descriptions of rotational collectivities of nuclei in the upper part of the  $0f_{7/2}$  shell (e.g.,  $^{48}\text{Cr}$ ) [31, 32, 33]. However, these interactions conserve isospin symmetry. In this work, we present a new isospin-nonconserving effective interaction derived microscopically from the underlying  $NN$  potential.

Traditionally, effective residual interaction is derived from phenomenal fit to observations [25] (e.g., the USD interaction for the  $sd$  shell.) or from the evaluation of the G reaction matrix [28]. Although the effective interaction can in principle be derived from true  $NN$  interaction, it has to be renormalized to include the contributions from the excluded configurations and to avoid the hard core of the bare  $NN$  potential. Renormalization methods have been proposed for the calculation of effective interaction from underlying meson-exchange potentials, like the momentum-space renormalization group decimation method ( $V_{\text{low-}k}$  approach) [34] and the unitary correlation operator method (UCOM) [35]. In  $V_{\text{low-}k}$  approach, high-momentum contributions are integrated out with the introduction of a cutoff, while

UCOM describes short-range correlations by a unitary transformation. In this paper, we used the so-called folded-diagram expansion method in which it is more convenient to include effects from excluded configurations. The folded-diagram expansion is a time-dependent perturbation theory introduced by Kuo *et al.* for the evaluation of residual interactions microscopically from bare  $NN$  potentials [23, 36]. The short-range repulsion is taken into account by the introduction of G matrix.

The folded (time-incorrect) and non-folded (time-correct) diagrams are introduced in the evaluation of the time-evolution operator  $U(0, -\infty)$  which can be written using perturbation expansion in the complex-time limit as,

$$U(0, -\infty) = \lim_{t \rightarrow -\infty(\varepsilon)} \sum_{n=0}^{\infty} \frac{1}{n!} \left(\frac{-i}{\hbar}\right)^n \int_t^0 dt_1 \int_t^0 dt_2 \cdots \int_t^0 dt_n T[H_1(t_1), H_1(t_2) \cdots H_1(t_n)], \quad (5)$$

where  $\lim_{t \rightarrow -\infty(\varepsilon)} \equiv \lim_{\varepsilon \rightarrow 0+} \lim_{t \rightarrow -\infty(1-i\varepsilon)}$  and  $T$  is the time-ordering operator in degenerate or nearly degenerate systems. For a model-space with the dimension  $D$ , the lowest  $D$  eigenstates of the true Hamiltonian can be constructed using the time-evolution operator with model-space states,  $\Phi_i$ ,

$$\lim_{t \rightarrow -\infty(\varepsilon)} \frac{U(0, -\infty)|\rho_\lambda\rangle}{\langle \rho_\lambda | U(0, -\infty) | \rho_\lambda \rangle} = \frac{|\Psi_\lambda\rangle}{\langle \rho_\lambda | \Psi_\lambda \rangle}, \quad (6)$$

where  $\lambda = 1, 2, \dots, D$  and  $|\rho_\lambda\rangle$  is a set of  $D$  parent states defined as

$$|\rho_\lambda\rangle = \sum_{i=1}^D C_i^{(\lambda)} |\Phi_i\rangle, \quad \lambda = 1, 2, \dots, D. \quad (7)$$

In the folded-diagram decomposition procedure, the wave function  $U(0, -\infty)|\Phi_i\rangle$  can be factorized as

$$U(0, -\infty)|\Phi_i\rangle = U_V(0, -\infty)|\Phi_i\rangle \times U(0, -\infty)|c\rangle, \quad (8)$$

where  $|c\rangle$  denotes the core and the subscript  $V$  means that all interactions in  $U_V(0, -\infty)$  are linked to valence particles. Moreover, diagrams contained in  $U_V(0, -\infty)|\Phi_i\rangle$  can be expressed in terms of so-called  $\hat{Q}$ -boxes. The  $\hat{Q}$ -box is made up of non-folded diagrams which are irreducible and valence-linked [23]. It is defined as

$$\hat{Q}(\omega) = PH_1P + PH_1Q \frac{1}{\omega - QHQ} QH_1P, \quad (9)$$

where  $\omega$  is the energy of interacting nucleons. The exclusion operator  $Q$  appears due to the Pauli principle preventing interacting nucleons from scattering into states occupied already by other nucleons [36].

Using the generalized time ordering, the effective interaction  $v_{\text{eff}}$  can be expanded in terms of  $\hat{Q}$ -boxes:

$$v_{\text{eff}} = \hat{Q} - \hat{Q}' \int \hat{Q} + \hat{Q}' \int \hat{Q} \int \hat{Q} - \dots, \quad (10)$$

where  $\int$  denotes a folding sign imposing relative time constraints.  $\hat{Q}'$  is a set of  $\hat{Q}$ -boxes that have at least two  $H_1$  vertices attached to valence lines, satisfying  $d\hat{Q}'/d\omega = d\hat{Q}/d\omega$ . Correspondingly, the solution of Eq. (10) can be derived using an iteration procedure:

$$v_{\text{eff}}^{(n)} = \hat{Q} + \sum_{m=1}^{\infty} \frac{1}{m!} \frac{d^m \hat{Q}}{d\omega^m} \{v_{\text{eff}}^{(n-1)}\}^m, \quad (11)$$

where the energy dependence of the  $\hat{Q}$ -box can be removed.

In practical evaluations, non-folded diagrams are calculated firstly and summed to give the  $\hat{Q}$ -box. To treat the strong repulsive core of the bare  $NN$  potential which is unsuitable for perturbation treatments, the Brueckner  $G$  reaction matrix is usually used. The  $\hat{Q}$ -boxes can be expressed in terms of  $G$ -matrix vertices. The  $G$  matrix is defined by the solution of the Bethe-Goldstone equation [36],

$$G = V + V \frac{\mathcal{Q}}{\omega - \mathcal{Q} H_0 \mathcal{Q}} G, \quad (12)$$

satisfying

$$\langle \Psi | G | \Psi \rangle = \langle \Psi | V | \Psi \rangle, \quad (13)$$

where  $\Psi$  is the correlated two-body wave function.

In the past decade, various high-precision phenomenological meson-exchange potentials have been proposed with reasonable descriptions of the charge symmetry breaking and charge independence breaking [22]. Initiated by Weinberg [37], the chiral perturbative  $NN$  potential derived from the low energy effective Lagrangians of the QCD model shows another promising way. All the potentials have similar low-momentum behavior. In the present work, the bare  $NN$  potential  $V$  is taken to be a new charge-dependent version of the Bonn one-boson-exchange potential as described in Ref. [22]. For further studies, theoretical works have also been carried out with a  $N^2LO$  chiral  $NN$  potential by Idaho group [37].

In the present work, we are interested in nuclei in the  $fp$  shell. The model space contains  $0f_{7/2}$ ,  $1p_{3/2}$ ,  $0f_{5/2}$ ,  $1p_{1/2}$  sub-shells with the core of  $^{40}\text{Ca}$ . The  $\hat{Q}$ -boxes are approximated to the third order. Single-particle energies are taken from the experimental excitation energies of the odd neutron in  $^{41}\text{Ca}$  [26]. In the CD Bonn potential, charge symmetry breaking

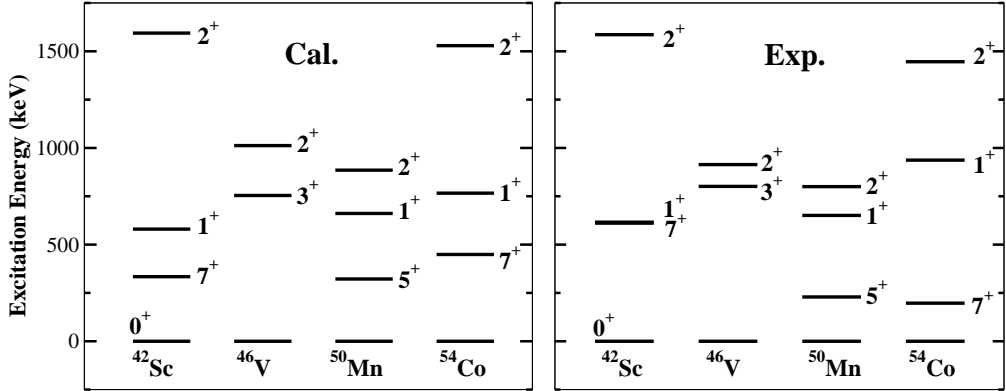


FIG. 1: Low-lying states in odd-odd  $N = Z$  nuclei in the  $0f_{7/2}$  shell. Calculated results and experimental data [38] are shown on the left-hand and right-hand side, respectively. All  $0^+$  ground states have the isospin of  $T = 1$ . The  $2^+$  levels shown are the first excited  $T = 1$  states.

$(V_{pp} \neq V_{nn})$  and charge independence breaking ( $V_{pp} \neq V_{pn} \neq V_{nn}$ ) effects are embedded in all partial waves with angular momentum  $J \leq 4$ . The contribution from the Coulomb field is also added when calculating the G matrix. The derived interaction is composed of three parts: the proton-proton, neutron-neutron and proton-neutron interactions. No specific mass dependence of the interaction is considered.

### III. LEVEL STRUCTURE

We calculated the level structures of odd-odd  $N = Z$  nuclei in the lower part of  $fp$  shell with the residual interaction derived as above. The effective Hamiltonian is diagonalized with the shell-model code OXBASH [39, 40]. The Hamiltonian matrix is given in proton/neutron formalism, with the neutrons and protons being naturally treated as two kinds of particles.

The calculations of low-lying states in odd-odd  $N = Z$  nuclei are shown in Fig. 1. For nuclei with mass number  $A \geq 50$ , calculations have been done in truncated  $fp$  model spaces. While the  $0^+$  and  $2^+$  states have  $T = 1$ , other states shown in Fig. 1 have  $T = 0$ . Isospin is not an explicit quantum number in our system. For a given state, the isospin quantum number is assigned through the detailed comparison with neighboring ( $T_z = \pm 1$ ) nuclei. Odd-odd  $N = Z$  nucleus and neighboring  $|T_z| = 1$  nuclei can form isospin triplet, leading to nearly identical  $T = 1$  bands. It can be seen that our calculations reproduce well the relative positions of the  $T = 1$  and  $T = 0$  states. The largest discrepancy compared with

experiments is seen for the  $7_1^+$  state in  $^{42}\text{Sc}$  where the core breaking effect that are not taken into account may be non-negligible. For the next heavier odd-odd  $N = Z$  nucleus,  $^{58}\text{Cu}$ , our calculation can reproduce well the near degenerating  $T = 1$  and  $T = 0$  bands, which are not shown in the figure. For heavier odd-odd  $N = Z$  nuclei, e.g.  $^{62}\text{Ga}$ , contributions from the  $0g_{9/2}$  sub-shell may become significant.

For comparison, we also used an interaction derived from the Idaho-A chiral  $NN$  potential [37] to calculate the low-lying states of the nuclei in Fig. 1. Similar results are obtained except  $^{42}\text{Sc}$  in which the calculated  $7^+$  state ( $T = 0$ ) is lower than the  $0^+$  state by about 47 keV in the Idaho-A potential.

As mentioned before, for nuclei in  $0f_{7/2}$  shell and above,  $T = 1$  ground states exist systematically. This situation has been studied by Satuła and Wyss [3] with an extended mean-field model in which the  $T = 1$  configuration is generated by isospin cranking. Based on the analysis of symmetry energy coefficients, the possible existence of isospin inversion has been extended to  $A = 96$  by Jänecke and O'Donnell [4]. In the shell-model Hamiltonian, different components of two-body interactions are mixed up. It is not easy to identify the role played by each component. One possible way is to separate contributions from so-called isovector and isoscalar pairing terms of the shell-model effective interaction [16]. Such an effort has already been tried [16]. In Ref. [16], authors argued that in the  $0f_{7/2}$  shell the competition between the isovector and isoscalar terms can lower the centroid of the  $T = 1$  state, leading to a  $T = 1$  ground state. The shell model could provide an efficient and qualitative way to search the interplay between various pairing correlations on the isospin structures of self-conjugate nuclei. The detailed evaluations of these terms would be done in future.

Tentative calculations have also been done for light nuclei in the  $p$ - and  $sd$ - shell. Results for odd-odd  $N = Z$  nuclei in these shells are encouraging, showing that the folded-diagram method is valid and efficient for the evaluation of shell-model interaction from  $NN$  potentials. It has long been a challenging problem that previous realistic shell-model calculations cannot give the right  $3^+$  ground state in odd-odd  $N = Z$  nuclei  $^{10}_5\text{B}$  [28]. Our calculations in the  $psd$  shell with the CD-Bonn potential reproduce well the  $3^+$  ground state and other low-lying states.

Experiments have observed high-spin states in  $^{46}\text{V}$  and  $^{50}\text{Mn}$  up to the  $0f_{7/2}$  band termination [8, 9, 10, 11]. Our calculations give excellent agreement with experiments. Fig. 2

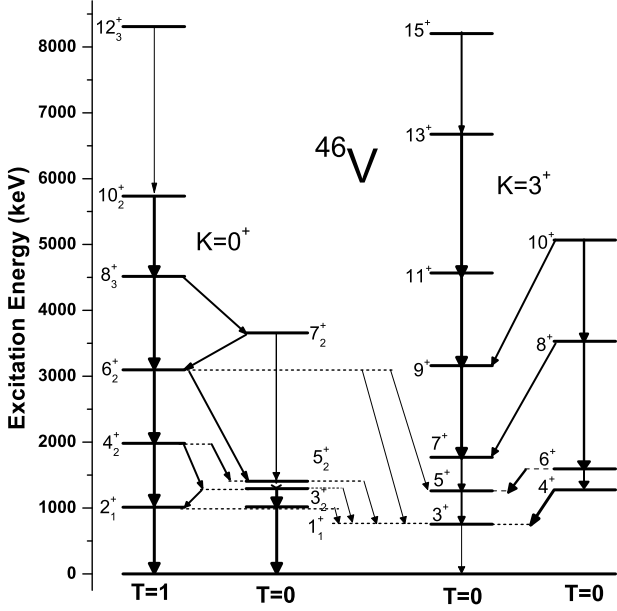


FIG. 2: Calculated level scheme in  $^{46}\text{V}$ . The comparison with experimental observations is shown in Fig. 3.

shows the calculated level scheme for  $^{46}\text{V}$ . Comparisons with experiments [11, 20] for  $T = 0$  and  $T = 1$  yrast bands are given in Fig. 3. The ground-state band has been assigned with the quantum number of  $K^\pi = 3^+$  and  $T = 0$  [10]. Recent experiments have deduced the  $T = 1$  ground-state bands in  $^{46}\text{V}$  and its isospin-triplet partners,  $^{46}\text{Ti}$  and  $^{46}\text{Cr}$ , up to  $J^\pi = 10^+$  [20]. Our calculations can reproduce the observations for the  $T = 1$  ground-state bands of these three nuclei. In  $^{46}\text{V}$ , a state with the excitation energy of  $E = 8267$  keV was detected and tentatively assigned as  $12^+$  by Garrett *et al.* [20]. The state corresponds to our calculated  $12_3^+$  state with the energy of 8309 keV in which the isospin quantum number was assigned as  $T = 1$ .

For the next heavier  $N = Z$  nucleus,  $^{50}\text{Mn}$ , we chose a truncation by allowing a maximum of two particles being excited to higher sub-shells above the  $f_{7/2}$  orbit. The truncation is valid since configurations for low-lying states are governed by the  $0f_{7/2}$  sub-shell. Fig. 4 gives calculated and experimental positive-parity states in  $^{50}\text{Mn}$ . The experiment [10] has identified the  $T = 0$  band up to the  $0f_{7/2}$  band termination and the  $T = 1$  band up to  $6^+$ . The observed  $8^+$  state at 4874 keV and  $10^+$  state at 6460 keV were assigned  $T = 0$  by O'Leary *et al.* [10]. Our calculations reproduce the  $T = 0$  and  $T = 1$  states.  $T = 1$  states

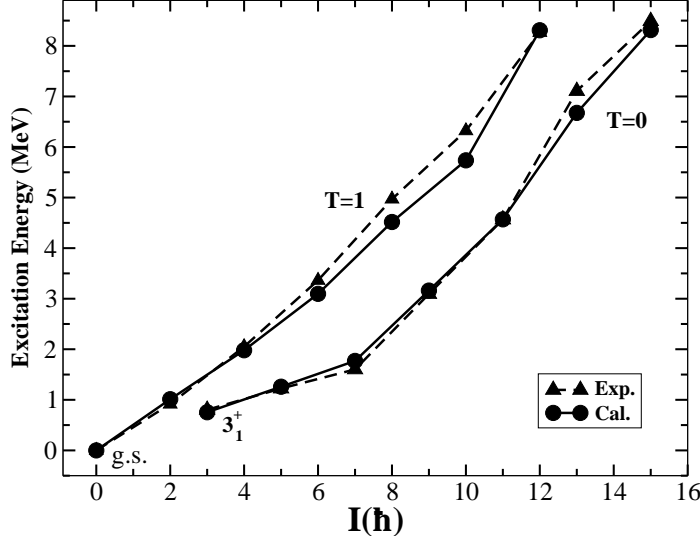


FIG. 3: Comparison between calculated and experimental  $T = 1$  and  $T = 0$  yrast bands in  $^{46}\text{V}$ . The experimental data are taken from Refs. [11, 20].

can be selected from the calculations of electrical quadrupole (E2) and magnetic dipole (M1) transition properties that will be discussed in the next section.

In the framework of the deformed Nilsson diagram, low-energy configurations in  $^{50}\text{Mn}$  have odd proton and odd neutron occupying the  $5/2^-$ [312] orbit of the  $0f_{7/2}$  sub-shell, leading to low-lying  $K^\pi = 0^+$  ( $T = 0$  or 1) and  $K^\pi = 5^+$  ( $T = 0$ ) configurations that have been identified experimentally [8, 12]. Our calculations have well reproduced the observed states, as shown in Fig. 4. Experiments observed that the  $K^\pi = 5^+$  state ( $T = 0$ ) is a  $T_{1/2} = 1.75$  m isomer with an excitation energy of 229 keV [8, 12]. Our calculation gives a energy of 322 keV for the isomer. Its decay is highly hindered due to the  $K$  selection rule. Low-lying metastable  $T = 0$  states also exist in other odd-odd  $N = Z$  nuclei shown in Fig. 1, due to large angular momentum gaps between  $0^+$  ground states and low-lying high-spin states. The  $K^\pi = 0^+$  band ( $T = 0$ ) in  $^{50}\text{Mn}$  has been observed with three members of  $1_1^+$ ,  $3_1^+$  and  $5_2^+$ , starting at the excitation energy of 651 keV for the  $1^+$  state. In present calculations, the lowest  $1^+$  state appears at 661 keV, forming a band as shown in Fig. 5. Also from the properties of inter-band M1 transition properties (discussed later), it can be obtained that the calculated band built on the  $1^+$  state corresponds for the observed  $K = 0^+$  band. The recent experiment [10] assigned new quantum numbers,  $J^\pi = 5^+$  and  $T = 0$ , for the observed state at 1917 keV. Our calculation confirms the  $5_2^+$  state with a calculated energy of 1813

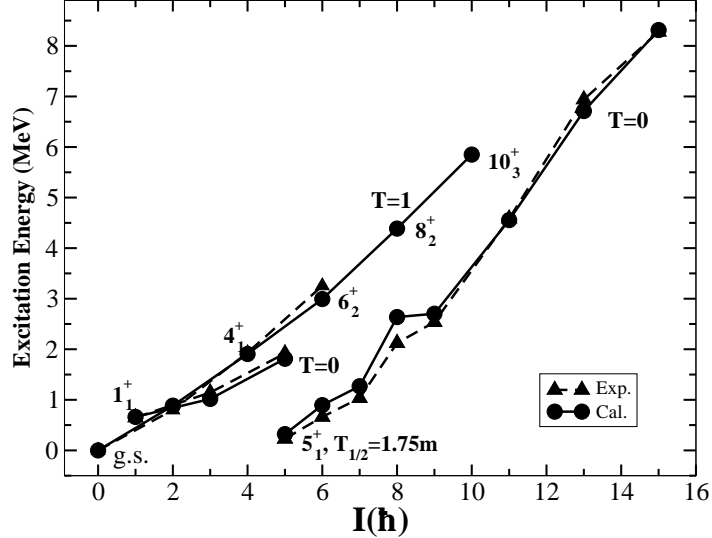


FIG. 4: Calculated and experimental [10] lowest  $T = 1$  and  $T = 0$  states in  $^{50}\text{Mn}$ . The  $T = 0$  states from  $5^+$  to  $15^+$  forms the  $K^\pi = 5^+$  band.

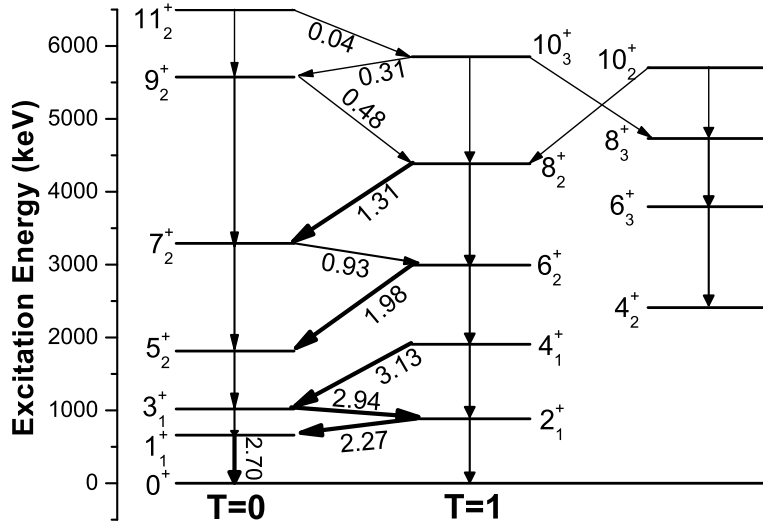


FIG. 5: Proposed isovector M1 transitions between the two  $K = 0^+$  bands in  $^{50}\text{Mn}$ . Calculated decay strengths (in  $\mu_N^2$ ) are shown along with the transition arrows.

keV.

Three negative-parity states with possible  $8^-$ ,  $10^-$  and  $12^-$  assignments were observed in  $^{50}\text{Mn}$  [9]. This band has been tentatively interpreted as an octupole vibration band coupled to the  $5_1^+$  isomeric state by Svensson *et al.* [9]. In the shell model, the negative-parity band could be generated in the  $sdfp$  shell with one particle exciting from the  $0d_{3/2}$  orbital.

#### IV. ELECTROMAGNETIC PROPERTIES

The electromagnetic (EM) transition properties of excited states can provide other detailed structure information. Particularly, EM properties play important roles in the identifications of various bands. In the following, we will investigate E2 and M1 transition properties in  $^{46}\text{V}$  and  $^{50}\text{Mn}$ , with a detailed analyse for  $^{50}\text{Mn}$ .

In practical shell-model calculations, transitions are treated in the truncated configuration. The wave functions ( $\Phi_\lambda$ ) of nuclear states are in fact the projections of the full-Hamiltonian wave functions ( $\Psi_\lambda$ ) onto the model space with introducing an effective interaction as described by Eq. (3). Hence, renormalized EM transition operators should be used to include effects from the excluded space,

$$\langle \Psi_f | \mathcal{O} | \Psi_i \rangle \longrightarrow \langle \Phi_f | \mathcal{O}_{\text{eff}} | \Phi_i \rangle, \quad (14)$$

where  $i$  and  $f$  indicate the initial and final states.

With the folded-diagram method, effective model-dependent transition operators can be derived microscopically [41, 42]. However, a simple way to evaluate the renormalization effect is to introduce the effective charges of nucleons [40]. For example, the effective operator for E2 transitions can be given as,

$$\mathcal{O}(\text{el.}, 2M) = \sum_i (\tilde{e}_\tau / e) r_i^2 Y_2^M(\theta_i, \phi_i), \quad (15)$$

where  $i$  sums over all particles and  $\tilde{e}_\tau$  (with  $\tau = \mu, \nu$ ) are renormalized effective charges for protons and neutrons, respectively.

Table I gives the shell-model predictions of  $\text{B}(\text{E2})$  values for  $K^\pi = 5^+$  and  $K^\pi = 0^+$  bands ( $T = 0$ ) in  $^{50}\text{Mn}$ . Two different groups of empirical effective charges have been used. One is the commonly-used effective charges of  $e_p = 1.5e$  and  $e_n = 0.5e$ . The other group with  $e_p = 1.15e$  and  $e_n = 0.80e$  was extracted from the  $\text{B}(\text{E2}; 27/2^- \rightarrow 23/2^-)$  values of  $T = 1/2$  mirror nuclei  $^{51}\text{Fe}$  and  $^{51}\text{Mn}$  by du Rietz *et al.* [43]. The wave functions of the shell model are calculated with three different bases, i.e., the harmonic oscillator (HO), the Woods-Saxon (WS) potential and the Skyrme force (SKcsb) by Brown *et al.* [44] in which a charge-symmetry-breaking term has been added. In the  $K = 5^+$  band ( $T = 0$ ) of  $^{50}\text{Mn}$ , one E2 strength has been determined [12]. The calculated  $\text{B}(\text{E2}, 9_1^+ \rightarrow 7_1^+)$  value agrees with the measured lower limit. As seen from Table I, calculated decay strengths are relatively

TABLE I: Calculated and observed B(E2) values (in  $e^2\text{fm}^4$ ) in  $^{50}\text{Mn}$ . Two groups of effective charges are used. One is the “standard” charges with  $e_p=1.50\text{e}$ ,  $e_n=0.50\text{e}$ ; the other one with  $e_p=1.15\text{e}$ ,  $e_n=0.80\text{e}$  taken from Ref. [43]. Experimental data are taken from Ref. [12].

$(J_i, T_i) \rightarrow (J_f, T_f)$	$e_p=1.50\text{e}, e_n=0.50\text{e}$			$e_p=1.15\text{e}, e_n=0.80\text{e}$			EXP
	HO	WS	SKcsb	HO	WS	SKcsb	
$K = 5^+$							
$(7_1^+, 0) \rightarrow (5_1^+, 0)$	45	42	37	42	39	35	
$(9_1^+, 0) \rightarrow (7_1^+, 0)$	151	143	126	142	133	118	$\geq 115^{+23}_{-19}$
$(11_1^+, 0) \rightarrow (9_1^+, 0)$	159	151	133	150	141	125	
$(13_1^+, 0) \rightarrow (11_1^+, 0)$	119	114	101	114	107	95	
$(15_1^+, 0) \rightarrow (13_1^+, 0)$	58	55	49	55	52	46	
$K = 0^+$							
$(3_1^+, 0) \rightarrow (1_1^+, 0)$	214	205	178	203	191	167	$700^{+240}_{-190}$
$(5_2^+, 0) \rightarrow (3_1^+, 0)$	189	182	158	180	170	148	$< 1880$
$(7_2^+, 0) \rightarrow (5_2^+, 0)$	168	163	141	160	151	132	
$(9_2^+, 0) \rightarrow (7_2^+, 0)$	85	83	71	81	77	67	
$(11_2^+, 0) \rightarrow (9_2^+, 0)$	4.5	4.4	3.9	4.3	4.1	3.7	

stable for different choices of effective charges and single-particle wave functions. Reduced E2 decay strengths for  $^{46}\text{V}$  are shown in Table II in which the results calculated with the HO single-particle wave function and effective charges of  $e_p=1.5\text{e}$  and  $e_n=0.5\text{e}$  are given.

Fig. 6 shows the calculations of electrical quadrupole transitions for the  $T = 1$  band in  $^{50}\text{Mn}$ . Results were calculated with  $e_p = 1.5\text{e}$  and  $e_n = 0.5\text{e}$  and HO single-particle wave functions. Three side bands identified experimentally are shown in the figure. Two bands with  $T = 0$  on the right side of the figure have been assigned with  $K^\pi = 3^+$  and  $K^\pi = 2^+$ , respectively, by Sahu *et al.* [45]. The proposed  $10_1^+$  state ( $T = 0$ ) at 5027 keV, and the  $8_2^+$  state ( $T = 1$ ) at 4386 keV have not been observed. Calculated  $8_3^+$  and  $10_2^+$  states are recognized as the observed  $8^+$  state at 4874 keV and the  $10^+$  state at 6460 keV, respectively. Both states have the isospin of  $T = 0$  since M1 transition strengths are rather weak compared with inner-band E2 transitions.

TABLE II: Calculated reduced transition strengths of M1 (in  $\mu_N^2$ ) and E2 (in  $e^2 \text{fm}^4$ ) transitions in  $^{46}\text{V}$ . Experimental data are taken from Refs. [17, 18].

$J_i \rightarrow J_f$	B(E2)		B(M1)	
	Cal.	Exp.	Cal.	Exp.
$K = 3^+$				
$5_1^+ \rightarrow 3_1^+$	29	67(14)		
$7_1^+ \rightarrow 5_1^+$	2	97(15)		
$9_1^+ \rightarrow 7_1^+$	173	159(34)		
$11_1^+ \rightarrow 9_1^+$	153	139(26)		
$13_1^+ \rightarrow 11_1^+$	109	78(16)		
$15_1^+ \rightarrow 13_1^+$	78	60(12)		
$4_1^+ \rightarrow 3_1^+$	280	208(50)	$4 \times 10^{-4}$	
$6_1^+ \rightarrow 5_1^+$	157		$9 \times 10^{-4}$	
$8_1^+ \rightarrow 7_1^+$	33		$2 \times 10^{-7}$	
$10_1^+ \rightarrow 9_1^+$	33		$3 \times 10^{-5}$	
$6_1^+ \rightarrow 4_1^+$	96			
$8_1^+ \rightarrow 6_1^+$	138			
$10_1^+ \rightarrow 8_1^+$	130			
$K = 0^+$				
$2_1^+ \rightarrow 0_1^+$	176	138(35)		
$4_2^+ \rightarrow 2_1^+$	237	> 169		
$6_2^+ \rightarrow 4_2^+$	221			
$8_3^+ \rightarrow 6_2^+$	212			
$10_2^+ \rightarrow 8_3^+$	161			
$12_3^+ \rightarrow 10_2^+$	0.03			
$3_2^+ \rightarrow 1_1^+$	217			
$5_2^+ \rightarrow 3_2^+$	117			
$7_2^+ \rightarrow 5_2^+$	0.07			
$\Delta K = 0, \Delta T = 1$				
$1_1^+ \rightarrow 0_1^+$			1.49	$\geq 0.77$
$3_2^+ \rightarrow 2_1^+$	0.05		1.14	2.0(7)
$4_2^+ \rightarrow 3_2^+$	0.15		1.0	0.57(15)
$4_2^+ \rightarrow 5_2^+$			1.26	0.55(13)
$6_2^+ \rightarrow 5_2^+$	0.11		0.33	
$7_2^+ \rightarrow 6_2^+$	0.12		0.03	
$8_2^+ \rightarrow 7_2^+$	3.7		0.06	
$\Delta K = 3, \Delta T = 1$				
$2_1^+ \rightarrow 3_1^+$	0.4		0.26	
$3_2^+ \rightarrow 3_1^+$	2.9		$2 \times 10^{-5}$	
$4_2^+ \rightarrow 3_1^+$			0.04	0.012
$4_2^+ \rightarrow 5_1^+$			0.236	0.02
$5_2^+ \rightarrow 3_1^+$	57			

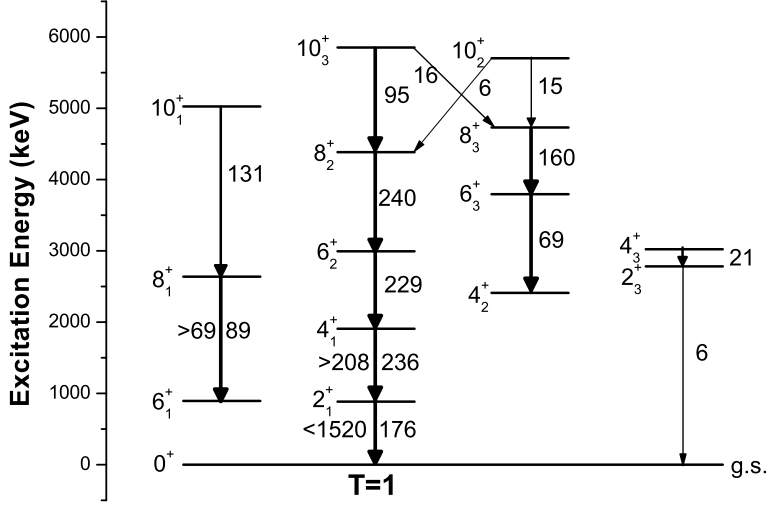


FIG. 6: Decay scheme and  $B(E2)$  strengths (in  $e^2\text{fm}^4$ ) of the proposed  $T=1$  band in  $^{50}\text{Mn}$ . Calculated and experimental strengths [12] are shown on the right- and left-hand sides of the transition lines, respectively.

The magnetic dipole (M1) operator is dominated by the isovector spin ( $\sigma$ ) term. Strong M1 transitions have been observed only in light nuclei. In the  $fp$  shell, due to the coexistence of  $T = 0$  and  $T = 1$  bands at low excitation energies, strong isovector ( $\Delta T = 1$ ) M1 transitions have been expected [10, 12]. We take the g-factor values of free nucleon and the HO basis to investigate the isoscalar and isovector M1 transition properties in  $^{46}\text{V}$  and  $^{50}\text{Mn}$ .

Part of calculated M1 transition strengths for  $^{46}\text{V}$  and  $^{50}\text{Mn}$  are shown in Table II and III, respectively. Available experimental data are given for comparison. Our calculations clearly show that  $\Delta T = 1$ , M1 transitions with  $\Delta K = 0$  are enhanced, while other  $\Delta T = 1$ , M1 transitions are retarded due to the  $K$  quantum number selection (M1 transitions with  $\Delta K \geq 1$  should be highly hindered). In  $^{46}\text{V}$ , four strong isovector M1 transitions have been observed. They were reproduced well in our calculations. In  $^{50}\text{Mn}$ , the uncertainty in experimental data is very large [12]. Calculated  $\Delta K = 0$  inter-band M1 transitions ( $\Delta T = 1$ ) are shown in Fig. 5. The strong M1 transitions have also been interpreted by a simple picture of quasideuteron configurations of odd neutron and odd proton in  $^{50}\text{Mn}$  [12].

Another exciting problem involving odd-odd  $N = Z$  nuclei is the study of super-allowed decays. The  $ft$  values of ground-state Fermi ( $0^+ \rightarrow 0^+$ ) decays would be the same for

TABLE III: Calculated reduced matrix elements (in  $\mu_N^2$ ) for M1 transitions in  $^{50}\text{Mn}$  with the g-factors of free nucleon [ $g_s(\text{proton})=5.586$ ,  $g_s(\text{neutron})=-3.826$ ,  $g_l(\text{proton})=1$  and  $g_l(\text{neutron})=0$ ]. Experimental data are taken from Ref. [12]. Calculated B(E2) values are also shown.

$(J_i, T_i) \rightarrow (J_f, T_f)$	B(E2)	B(M1)	
	Cal.	Cal.	Exp.
$\Delta T = 1$			
$(1_1^+, 0) \rightarrow (0_1^+, 1)$		2.70	
$(2_1^+, 1) \rightarrow (1_1^+, 0)$	0.28	2.27	$<6.7$
$(3_1^+, 0) \rightarrow (2_1^+, 1)$	$0.78 \times 10^{-2}$	2.94	$2.9_{-7}^{+10}$
$(4_1^+, 1) \rightarrow (3_1^+, 0)$	0.70	3.13	$1.05_{-20}^{+31}$
$(6_2^+, 1) \rightarrow (5_2^+, 0)$	1.46	1.98	$>0.24$
$(7_2^+, 0) \rightarrow (6_2^+, 1)$	0.30	0.93	
$(8_2^+, 1) \rightarrow (7_2^+, 0)$	1.66	1.31	
$(9_2^+, 0) \rightarrow (8_2^+, 1)$	$0.93 \times 10^{-2}$	0.48	
$(10_3^+, 1) \rightarrow (9_2^+, 0)$	0.43	0.31	
$(11_2^+, 0) \rightarrow (10_3^+, 1)$	3.76	0.04	
$\Delta T = 0$			
$(4_2^+, 0) \rightarrow (3_1^+, 0)$	2.0	$8.65 \times 10^{-5}$	
$(4_3^+, 0) \rightarrow (3_1^+, 0)$	0.34	$4.67 \times 10^{-2}$	
$(8_3^+, 0) \rightarrow (7_2^+, 0)$	7.5	$4.30 \times 10^{-4}$	
$(10_2^+, 0) \rightarrow (9_2^+, 0)$	0.08	0.023	
$(11_2^+, 0) \rightarrow (10_2^+, 0)$	35	0.06	

analogous transitions if the conserved vector current (CVC) hypothesis is valid [46]. Odd-odd  $N = Z$  nuclei provide the best ground to test the understanding of the electroweak interaction. As discussed in Ref. [46], the isospin-symmetry breaking effect has significant contribution on the asymmetry in analogous transitions. In our Hamiltonian, the isospin symmetry breaking is treated microscopically, which can provide a basis to quantify the effect. However, it is beyond the scope of this paper.

## V. CONCLUSION

A microscopical  $fp$ -shell interaction has been constructed from the high-precision CD Bonn  $NN$  potential using the folded-diagram renormalization method. In the CD Bonn potential, both charge symmetry breaking and charge independence breaking are well described. The Coulomb field is also included in calculating the effective interaction. Hence, in our effective Hamiltonian, isospin symmetry is naturally broken. The isospin-nonconserving interaction has been used to investigate the level structures of odd-odd self-conjugate nuclei in the lower part of  $fp$  shell. Excellent agreements between calculations and experiments have been obtained. Particularly, the interaction gave a good description of the isospin structures in odd-odd  $N = Z$  nuclei, reproducing well the relative positions of  $T = 0$  and  $T = 1$  bands. Further studies done with the Idaho-A chiral perturbation potential showed similar results. Moreover, calculations show that effective interactions derived with the folded-diagram method can reproduce the low-lying structures of odd-odd  $N = Z$  nuclei in other major shells, including the famous case of  $^{10}_5\text{B}$  in  $p$  shell. Our calculations reproduce the high-spin isomeric states in the  $fp$  shell. In particular, we have performed detailed shell-model calculations for the positive-parity states in  $^{46}\text{V}$  and  $^{50}\text{Mn}$ . EM transition properties and isospin structures in odd-odd  $N = Z$  nuclei have been predicted and discussed. We can construct a one-to-one correspondence between calculated results and experimental data with the comparisons of excitation energies and electromagnetic transition properties. Our study shows that the predictions of this *ab initio* interaction is encouraging. It is very interesting to test its performance in other  $fp$  shell nuclei. Further studies will be carried out in our future works.

### Acknowledgement

The authors are grateful to Prof. B.A. Brown for providing us the code OXBASH on the request. This work has been supported by the Natural Science Foundations of China under Grant Nos. 10525520 and 10475002, the Key Grant Project (Grant No. 305001) of Ministry of Education of China. We also thank the PKU computer Center where numerical

calculations have been done.

---

- [1] D.J. Dean and M. Hjorth-Jensen, Rev. Mod. Phys. **75**, 607 (2003).
- [2] A.O. Macchiavelli, *et al.*, Phys. Rev. C **61**, 041303(R) (2000).
- [3] W. Satuła and R. Wyss, Phys. Lett **B393**, 1 (1997); Phys. Rev. Lett **86**, 4488 (2001).
- [4] J. Jänecke and T.W. O'Donnell, Phys. Lett. **B605**, 87 (2005), and reference therein.
- [5] P. Vogel, Nucl. Phys. A **662**, 148 (2000).
- [6] I. Schneider, *et al.*, Phys. Rev. C **61**, 044312 (2000).
- [7] C. Friebner, *et al.*, Phys. Rev. C **60**, 011304 (1999).
- [8] A. Schmidt, *et al.*, Phys. Rev. C **62**, 044319 (2000).
- [9] C.E. Svensson, *et al.*, Phys. Rev. C **58**, R2621 (1998).
- [10] C.D. O'Leary, *et al.*, Phys. Lett. **B525**, 49 (2002).
- [11] C.D. O'Leary, *et al.*, Phys. Lett. **B459**, 73 (1999).
- [12] N. Pietralla *et al.*, Phys. Rev. C **65**, 024317 (2002).
- [13] S. Skoda, *et al.*, Phys. Rev. C **58**, R5 (1998).
- [14] S.M. Lenzi, *et al.*, Phys. Rev. C **60**, 021303 (1999).
- [15] A. Petrovici, K.W. Schmid, and A. Faessler, Nucl. Phys. **A647**, 197 (1999).
- [16] A. Poves and G. Martínez-Pinedo, Phys. Lett. **B430**, 203 (1998).
- [17] F. Brandolini *et al.*, Phys. Rev. C **64**, 044307 (2001).
- [18] P. von Brentano *et al.*, Nucl. Phys. **A682**, 48c (2001).
- [19] S.M. Lenzi *et al.*, Phys. Rev. Lett. **87**, 122501 (2001).
- [20] P.E. Garrett *et al.*, Phys. Rev. Lett. **87**, 132502 (2001).
- [21] A.P. Zuker, S.M. Lenzi, G. Martínez-Pinedo, and A. Poves, Phys. Rev. Lett. **89**, 142502 (2002).
- [22] R. Machleidt, Phys. Rev. C **63**, 024001 (2001).
- [23] T.T.S. Kuo and E. Osnes, Folded-Diagram Theory of Effective Interaction in Nuclei, Atoms and Molecules, Springer Lecture Notes in Physics, Vol. 364 (Springer-Verlag, Berlin, 1990).
- [24] S. Cohen and D. Kurath, Nucl. Phys. **73**, 1 (1965).
- [25] B.H. Wildenthal, Prog. Part. Nucl. Phys. **11**, 5 (1984).
- [26] T.T.S. Kuo and G.E. Brown, Nucl. Phys. **A114**, 241 (1968).

- [27] A. Poves and A. Zuker, Phys. Rep. **70**, 235 (1981).
- [28] E. Caurier, G. Martínez-Pinedo, F. Nowacki, A. Poves, and A.P. Zuker, Rev. Mod. Phys. **77**, 427 (2005).
- [29] W.A. Richter, M.G. van der Merwe, R.E. Julies, and B.A. Brown, Nucl. Phys. **A704**, 134 (1991).
- [30] M. Honma, T. Otsuka, B.A. Brown, and T. Mizusaki, Phys. Rev. C **65**, 061301(R) (2002).
- [31] E. Caurier, A.P. Zuker, A. Poves, and G. Martínez-Pinedo, Phys. Rev. C **50**, 225 (1994).
- [32] E. Caurier *et al.*, Phys. Rev. Lett. **75**, 2466 (1995).
- [33] G. Martínez-Pinedo, A.P. Zuker, A. Poves, and E. Caurier, Phys. Rev. C **55**, 187 (1996).
- [34] S.K. Bogner, T.T.S. Kuo, and A. Schwenk, Phys. Rep. **386**, 1 (2003).
- [35] H. Feldmeier, T. Neff, R. Roth, and J. Schnack, Nucl. Phys. A **632**, 61 (1998).
- [36] M. Hjorth-Jensen, T.T.S. Kuo, and E. Osnnes, Phys. Rep. **261**, 125 (1995).
- [37] D.R. Entem and R. Machleidt, Phys. Lett. **B524**, 93 (2002).
- [38] *Table of Isotopes*, 8th ed., edited by R.B. Firestone and V.S. Shirley (Wiley, New York, 1996) Vol. 2.
- [39] A. Etchegoyen, W.D.M. Rae, N.S. Godwin, W.A. Richter, C.H. Zimmerman, B.A. Brown, W.E. Ormand, and J.S. Winfield, MSU-NSCL Report No. 524 (1985).
- [40] B.A. Brown, Prog. Part. Nucl. Phys. **47**, 517 (2001).
- [41] T. Siiskonen, M. Hjorth-Jensen, and J. Suhonen, Phys. Rev. C **63**, 055501 (2001).
- [42] T. Engeland, M. Hjorth-Jensen, and E. Osnnes, Phys. Rev. C **61**, 021302 (2000).
- [43] R. du Rietz *et al.*, Phys. Rev. Lett. **93**, 222501 (2004).
- [44] B.A. Brown, W.A. Richter, and R. Lindsay, Phys. Lett. **B483**, 49 (2000).
- [45] R. Sahu and V.K.B Kota, Phys. Rev. C **67**, 054323 (2003).
- [46] J.C. Hardy and I.S. Towner, Phys. Rev. C **71**, 055501 (2005).